A Low-Cost, Nanowatt, Millimeter-Scale Memristive-Vacuum Sensor

Khaled Humood, Sueda Saylan, Baker Mohammad, and Maguy Abi Jaoude

***Abstract*— This work demonstrates a low-power, light-weight, and cost-efficient vacuum pressure sensor and air leak detector based on 2 mm x 2 mm $Cu/HfO_2/p^+$-Si memristor device. The operating principle of the proposed sensor relies on monitoring the off-state resistance (R_{off}) of the device, wherein the experimental results show that the R_{off} value is inversely proportional to the vacuum pressure. The fabricated sensors demonstrated a sensitivity of 493 $Torr^{-1}$ and power consumption as low as ~ 8 nW, when tested in a wide range of sub-atmospheric pressure ($4.9x10^{-5}$ – 760) Torr, making them highly suitable for low-power applications. Furthermore, it is shown that the sensor can be integrated with a microcontroller-based circuitry to serve as a standalone sensing system.**

***Index Terms*—vacuum sensor, air leak detector, memristor, ReRAM.**

I. Introduction

Air leaks pose a significant concern for pressurized space structure integrity and astronaut safety [1]. Micrometeoroids and orbital debris (MMOD) with diameters ranging from 25 mm to 125 mm, and traveling at approximately 9-10 km/s in the Low Earth Orbit (LEO) frequently impact and damage the International Space Station (ISS) and other space-based structures [1, 2]. Moreover, this is nowadays becoming a severe threat as the number of MMODs in the LEO increases due to accelerated space mission programs [3]. Therefore, continuous monitoring of air leaks is needed and this requires low-power, low-weight vacuum pressure sensing systems.

Pressure sensors are widely used in space pressurized structures and environments. Various solutions in the literature enable to sense changes in the pressure from the atmospheric pressure (~760 Torr) down to high vacuum ($\sim 6.5 \times 10^{-6}$ Torr) [4-11]. These solutions are thermal sensors that depend on the heat transfer principle [7-11], or they rely on frequency shifts caused by damping variation under different pressures [4-6]. However, most of the proposed solutions operate at high power and require heavy and oversized circuitry to be used (see Table II), not being able to comply with low power, light weight, and small footprint requirements for mobile applications [1, 2].

In this work, a novel low-cost, small-form-factor, and low-power vacuum pressure sensor, based on 2 mm x 2 mm Cu/HfO_2(~ 80-nm-thick)/p^+-Si memristor devices, is proposed for the potential development of air-leak sensors. Furthermore, a complete system implementation using an Arduino microcontroller that is compatible with the low-power and small-area targets of the application is presented.

Emerging memristor (MR) technologies play an important role in electronic applications due to their low-power operation, small footprint, multi-level and high-speed switching behavior [12-14]. The two-terminal structure of memristive devices enables the integration of high dense crossbar arrays with a minimal bit area of $4F^2$, where F is the minimum feature size [15]. The resistive switching (RS) property in MRs has also been exploited in applications beyond memory, such as matrix multiplication, in-memory computing (IMC), and hardware-accelerated processing [16-19]. Moreover, the capability of the MR electrical parameters to respond to external stimuli is promising for expanding the use of memristors as sensing elements [20-22]. Further, the intrinsic variability in MR electrical characteristics, from cycle to cycle and from device to device, could be exploited for security applications [23-25].

The proposed sensor utilizes the change in the off-state resistance (R_{off}) of the memristor in response to a change in the pressure, to sense a transition from the atmosphere to vacuum environment. Such a sensing method does not depend on temperature or frequency changes, and hence it is less susceptible to noise and interference [4]. Furthermore, the utilization of R_{off} as the basis of sensing leads to extremely low power consumption, as low as 8 nw . Compared with the state-of-the-art (see Table II), the proposed sensor provides more than three orders of magnitude improvement in the power consumption, making the sensor critically important for low power applications. Moreover, the sensor makes use of a light-weight and low-power circuity based on Arduino micro-controller, eliminating the need for heavy and expensive equipment such as amplifiers, function generators, spectrum analyzers.

Device fabrication, performance characterization, and circuit implementation of the memristor-based vacuum sensor are described in detail in the following sections.

This work was supported in part by the UAE Space Agency under the Grant K08 2016 001. Additional support was received from Khalifa University System on Chip Center (SoCC) under the Grant RC2 2018-020.

K. H. Author was with SoCC and now with Electronics and Computer Science, University of Southampton, Southampton, United Kingdom. (email: khaledm.humood@gmail.com) S. S. and B. M. Authors are with the System on Chip Center and Electrical Engineering and Computer Science Department at Khalifa University of Science and Technology, Abu Dhabi, UAE (sueda.saylan@gmail.com, baker.mohammad@ku.ac.ae). M. A. J. Author is with the Chemistry Department at Khalifa University of Science and Technology, Abu Dhabi, UAE (email: maguy.abijaoude@ku.ac.ae).

II. Materials And Methods

A. Device Fabrication

Fig. 1(a) shows the schematic representation and top view photograph of the fabricated devices, where the Cu top electrode (TE) defines the effective area for one device. The Cu TE was deposited by DC sputtering using a Q300T T coating system (Quorum Technologies, UK). The details of the HfO_2 deposition, as well as a comprehensive electrical characterization and statistical data analysis for the devices, can be found in [20, 26].

B. Experimental Setup

Fig. 1(b) and **Fig. 1(c)** show the experimental setup used for measuring the device resistance in alternating atmospheric and vacuum conditions. The setup consists of a cryogenic vacuum probe station (TTPX, Lake Shore Cryotronics Inc., USA) and a parameter analyzer (Keithley 2450, Tektronix, USA). The sensor is placed inside the vacuum chamber of the probe station (Fig. 1(b)) and its off-state resistance R_{off} is measured using the parameter analyzer that is connected to the probe arm base of the probe station (Fig. 1(c)). The details of the R_{off} read operation are given in Section II.D. A turbo pumping system (X3580A, Agilent Technologies, Switzerland) is used to control and read the pressure in the system.

C. I-V Characterization

The Current-Voltage *(I-V)* characteristics were obtained using a Keithley 4200-SCS parameter analyzer, by applying DC linear sweep functions. Dual positive sweeps ranging from 0 to 3.5 V and 0 to - 3.5 V were applied for the SET and RESET operations, respectively, with a voltage step size of 0.05 V in both cases. The p^+-Si bottom electrode was grounded during both operations. These measurements were performed at room temperature and in ambient air. This procedure was used to pre-screen the memristor characteristics and is not required when the device is deployed in the intended application. An account of the material and electrical characterization studies of the devices under atmospheric and vacuum environment is reported elsewhere [26].

D. R_{off} Read Operation

The R_{off} read operation illustrated in Fig. 2 was performed by using the experimental setup described in Section II.B. A read pulse was applied every 30 seconds to take a resistance measurement. The pulse amplitude was set to -0.4 V with a duration of 60 µs, which is the minimum pulse duration applicable by the tool. The read pulse magnitude and polarity were selected to minimize any changes in the resistance state of the device due to the read operation.

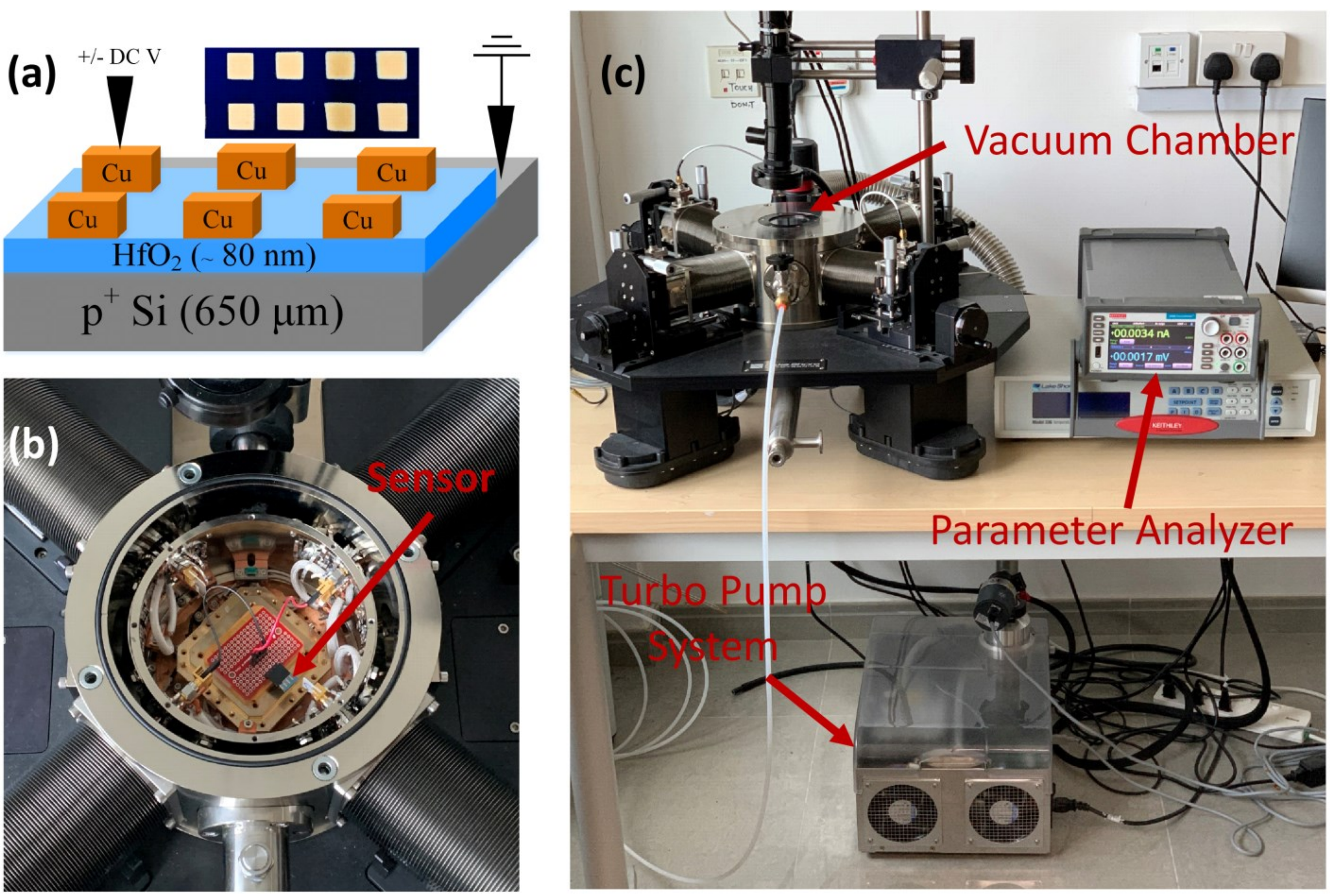

Fig. 1. (a) Schematic representation and top view photograph of the fabricated $Cu/HfO_2/p^+$-Si devices, where each Cu electrode (2 mm x 2 mm) defines a single device. The Cu electrode is supplied with a DC voltage, while the silicon electrode is grounded. Photograph of the experimental setup used for measuring the device resistance in alternating atmospheric and vacuum conditions, showing (b) the sensor prototype on a breadboard and (c) the vacuum chamber, parameter analyzer, and turbo pumping system.

III. Results and Discussion

A. Resistive Switching and Capacitance Characteristics of Cu/HfO_2/p^+-Si Devices in Air Atmosphere

Fig. 3 shows a pristine device tested through consecutive 10 SET-RESET voltage sweeps in the air atmosphere, to verify the cycle-to-cycle stability before investigating the vacuum sensing performance. In agreement with our previous findings [20], the device exhibited bipolar resistive switching within a bias voltage sweep window of +3.5 to -3.5 V and did not require an electroforming step, which is typical for the devices operating under the ECM mechanism [27, 28]. During the SET sweeps, a compliance current I_{CC} = 500 μA was maintained to avoid the permanent breakdown of the dielectric material of the device [29, 30]. A detailed investigation of the device-to-device and cycle-to-cycle variation of the Cu/HfO_2/p^+-Si device characteristics can be found in our previous work [20, 26]. In addition, the capacitance characteristics of the device for the HRS and LRS are shown in the Supplementary Material, Fig. S1.

B. Vacuum Behavior of Cu/HfO_2/p^+-Si Devices

After screening the devices in the air atmosphere (Fig. 3), the electrical characterization was performed in alternating air and vacuum conditions to investigate the performance of the developed technology as a vacuum pressure sensor. In particular, we measured the off-state resistance R_{off} by executing the read operation described in Section II.D. Fig. 4 shows the device R_{off} as a function of vacuum pressure ranging from ~ 3.2 x 10^{-3} to 4.9 x 10^{-5} Torr while the turbo pumping system evacuates the vacuum chamber. Before evacuating the testing chamber, the resistance was measured in the air atmosphere for 10 min and recorded to be ~ 27 MΩ as shown in the Supplementary Material Fig. S2. After starting the turbopump, the resistance increased gradually as the pressure reduced until a pressure threshold value P_{th}= 5.5 x 10^{-5} Torr (see Fig. 5(a) for the range of experimentally recorded P_{th}), at which an abrupt increase in the resistance from 39 MΩ to 126 MΩ was observed.

Thus, in response to a change in vacuum pressure, the off-state resistance exhibited two distinct regimes: first, the resistance gradually increased as shown in the inset of Fig. 4, following the power equation shown in the inset; and second, it abruptly increased beyond the threshold pressure P_{th}. This allows the use of the developed technology as a vacuum pressure sensor in the first region and as a vacuum detector in the latter. The resistance versus time plot of the data presented in Fig. 4 is shown in the Supplementary Material, Fig. S2. In addition, the R_{off} response of another pristine device as a function of pressure (Fig. S3), as well as the response of the device to pressure changes between atmosphere and vacuum over multiple cycles (Fig. S4) are provided in the Supplementary Material. The data presented in Fig. S4 show that the time response of the proposed sensor during the pumping stage (i.e., when the pressure changes from atmospheric to vacuum pressure levels) is not equivalent to the time response for the venting stage (i.e., when the pressure changes from vacuum to atmospheric). Hence, the proposed sensor can be utilized in vacuum sensing and detection applications wherein the pressure only changes in one direction

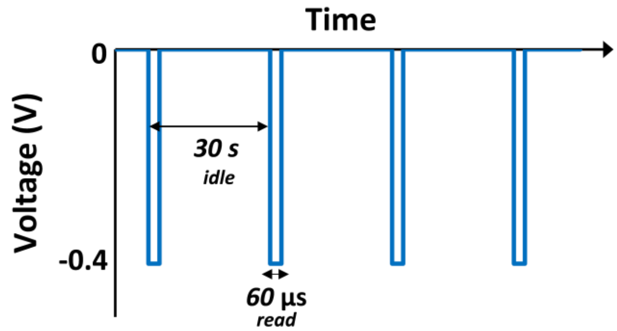

Fig. 2. R_{off} read pulses. The read voltage amplitude and the read period were set to -0.4 V and 30 s, respectively. The pulse width was set to 60 µs, which is the minimum width achievable by our setup.

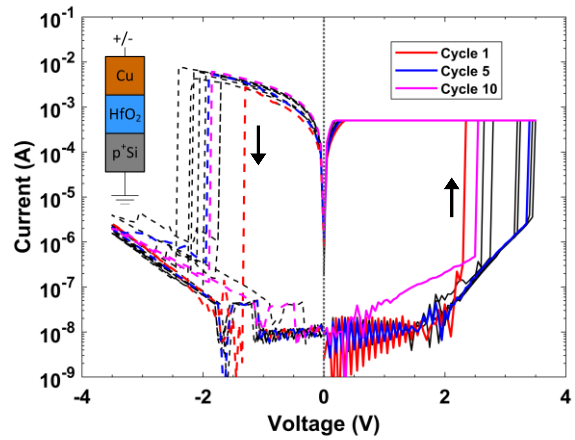

Fig. 3. *I-V* characteristics for SET (solid lines) and RESET (dashed lines) of a Cu/HfO_2/p^+-Si device programmed using a compliance current of 500 µA. Cycles 1, 5, and 10 are highlighted in red, blue, and magenta, respectively. Other cycles are highlighted in black. The arrows indicate the direction of current. The biasing scheme is shown in the inset.

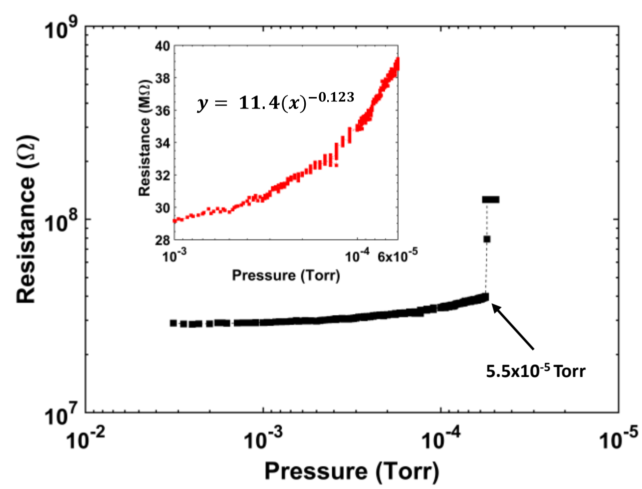

Fig. 4. R_{off} as a function of pressure from 3.2x10^{-3} to 4.9x10^{-5} Torr. The resistance was measured as 29 MΩ and 126 MΩ at 3.2x10^{-3} and 4.9x10^{-5} Torr, respectively. Prior to the measurements in vacuum, the atmospheric off-state resistance was measured to be R_{off}^{atm} = 27 MΩ. The inset shows the change in resistance as a function of pressure from 1x10^{-3} to 6x10^{-5} Torr. The sensitivity within this pressure range is 493 $Torr^{-1}$. Note: the x-axis values are reversed.

from atmospheric to vacuum. Moreover, Fig. S4 shows that the sensor could be reused for vacuum detection after the relaxation time in atmosphere has passed.

Furthermore, to confirm that the change in R_{off} is due to a change in the vacuum pressure but not due to electrical biasing over a long period, the resistance of a pristine device was measured over 70 hours at atmospheric pressure (760 Torr) as shown in the Supplementary Material, Fig. S5. As demonstrated by the results, the off-state resistance did not change during this experiment.

The sensitivity of the vacuum pressure sensor in the gradual region was calculated using the formula:

$$S = \frac{\Delta R_{off}/R_{off_i}}{\Delta p}, \quad (1)$$

where ΔR_{off} is the change in resistance, R_{off_i} is the initial resistance in air and Δp is the change in pressure [31]. Based on the data presented in Fig. 4, the sensitivity is ~ 493 $Torr^{-1}$ in a pressure range from $1x10^{-3}$ to $6x10^{-5}$ Torr. Utilizing the change in R_{off} as the quantitative parameter for sensing significantly reduces the power consumption. The R_{off} values of the fabricated devices lie in the range of 20-200 MΩ. At a read voltage of $V_{read} = 0.4$ V, the maximum power is estimated to be ~ 8 nW by using (2).

$$Power = \frac{V_{read}^2}{R_{off}} \quad (2)$$

Fig. 5(a) shows the device-to-device distribution of the pressure threshold P_{th} versus the ratio of R_{off} values measured in vacuum (R_{off}^{vac}) at P_{th} and in air atmosphere (R_{off}^{atm}). Each data point represents an individual device, presenting the data for 24 devices in total. Figure 5(b) shows the cumulative distribution function (CDF) of the ratio $R_{off}^{vac} / R_{off}^{atm}$, which is defined as the probability that the random variable *X,* corresponding to the resistance ratio in this case, assumes a value less than or equal to a given *x*. That is, *F(x)* is the probability that the resistance ratio will be less than or equal to *x*, whereas, *1 − F(x)* is the probability that the ratio will be greater than *x*. As seen in Fig. 5(a), most devices exhibited a resistance ratio above 2 at the measured pressure threshold P_{th} values. Based on the CDF plotted in Fig. 5(b), the probability that the resistance ratio will be greater than 2 is estimated at ~ 83%. This result indicates that the measured resistance ratio of the $Cu/HfO_2/p^+$-Si memristive devices can be used as a reliable metric to distinguish a measurable change in the ambient pressure between atmosphere and vacuum.

C. Sensing Principle

The vacuum pressure sensing mechanism by $Cu/HfO_2/p^+$-Si memristor device relies on a change in the electronic current conduction in the HRS. As shown in Fig. 6(a) and Fig. 6(b), respectively, the device involves two Schottky barriers connected back-to-back with a series resistance [32, 33] and the current conduction at HRS follows the Schottky emission, as evidenced by a linear dependence of *ln(I)* on $V^{1/2}$ [34]. The current-voltage data presented in Fig. 6(b) have been extracted from the *I-V* sweeps performed in air and vacuum by using the same device in both cases (Supplementary Material Fig. S6). The bias voltage range (0.2 - 1 V) is selected to be less than the SET voltage to ensure that the device is in the HRS. The regression equations obtained for the linear fits to the data (*solid lines*) are also provided in Fig. 6(b). The slope (*a*) and the

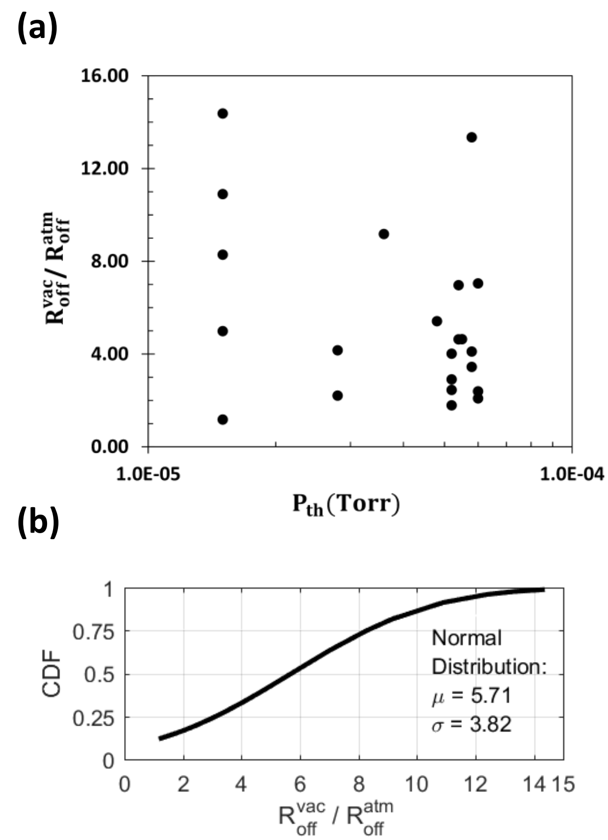

Fig. 5. (a) Device-to-device distribution of the threshold pressure (P_{th}), along with the ratio of R_{off} values measured in atmosphere (R_{off}^{atm}) and in vacuum (R_{off}^{vac}) after the threshold pressure is reached. Each data point represents an individual device. (b) Cumulative distribution function (CDF) fit of the resistance ratio, $R_{off}^{vac}/R_{off}^{atm}$.

y-intercept (*b*) of the linear regression equations (*y = ax + b*) are proportional to, respectively, the Schottky field-lowering coefficient (β_s) and the potential barrier at the interface under zero applied bias (φ_0) according to the Schottky emission equation [34]:

$$I = AT^2 \exp\left(-\frac{\varphi_0}{k_B T}\right) \exp\left(\frac{\beta_s V^{1/2}}{k_B T d^{1/2}}\right), \quad (3)$$

where the constant *A* is the product of area and Richardson constant, *T* the absolute temperature, k_B the Boltzmann constant, d the film thickness. The Schottky field-lowering coefficient β_s is given by

$$\beta_s = \left(\frac{e^3}{4\pi\varepsilon_r\varepsilon_0}\right)^{1/2}, \quad (4)$$

where ε_r is the relative permittivity of the material, ε_0 the permittivity of free space. The linear regression equations similarly obtained for two other devices (D2 and D3) are also listed in Table I.

A comparison of the slope *a* allows the comparison of β_s for different devices and different ambient conditions, wherein different β_s values imply different relative permittivity of the HfO_2 film. Similarly, a comparison of the y-intercept *b* allows the comparison of the potential barrier φ_0. As seen in Table I, *a* and *b* can be different for different devices under the same ambient conditions, indicating the formation of different interface products and/or different formation amounts, as well as the formation of different bonding structures and molecules

TABLE I
LINEAR REGRESSION PARAMETERS FIT TO THE LN(I) VERSUS $V^{1/2}$ DATA OBTAINED FOR DIFFERENT DEVICES IN ATMOSPHERE AND VACUUM

$y = ax + b$	Atmosphere			Vacuum		
	a	b	R^2	a	b	R^2
D1	5.4	- 20.48	0.9998	5.5	- 21.85	0.9992
D2	6.5	- 17.52	0.9932	4.3	- 17.73	0.9971
D3	4.5	- 15.66	0.9923	3.2	- 15.78	0.9949

in the HfO_2 film in individual devices, during the electrical biasing. In addition, these structural variations may be existent in the as-fabricated devices to an extent. For D2 and D3, a is diminished in vacuum, suggesting a decrease in the field-lowering coefficient β_s and thus an increase in the relative permittivity ε_r of the HfO_2 film, while it remains almost the same for D1. On the other hand, b, which is proportional to φ_0, increased in vacuum for all three devices, suggesting an increase in the barrier height to be the main source of reduced current conduction in vacuum. It can additionally be argued that compositional changes may have also occurred in the HfO_2 film, linked to the changes at the electrode interface that have led to an increase in the barrier height. Thus, a change in the series resistance of the HfO_2 film may also be playing a role in the changing electronic transport in vacuum.

Functional groups can play an essential role in the operation of memristive devices [35-37]. For instance, recently, a type of memristor that is based on the proton movement and proton-coupled electron transfer (PCET) processes has been reported [35], wherein the proton conductivity has increased with increasing humidity and this has led to a strong dependence of *I-V* plots on the humidity. In another study, it is reported that the OH^- groups attached on the lateral surfaces of ZnO nanowires is responsible for altering the Schottky barrier at the electrode/ZnO interface and decreasing the overall electronic conductivity in a memristive nanowire [36]. It was also shown by means of ab initio density functional theory (DFT) calculations that the OH^- groups, as well as $CH_3\text{-}O^-$ and $CH_3\text{-}COO^-$, cause deep surface states to form at the top of the ZnO valence band that act as electron traps and thus reduce the nanowire conductivity [37]. As we have shown earlier [26], the FT-IR spectrum for a vacuum-tested Cu/HfO_2/p^+-Si device (subjected to electrical biasing in vacuum) can be quite different from that of a pristine sample (not subjected to electrical biasing and vacuum conditions). While the distinct symmetric stretching vibrations for carboxylate groups (COO^-) and carbonate species were present only in the vacuum-tested device, the representative FT-IR absorption bands for stretching vibrations of water molecules were substantially present only in the pristine device. As suggested in the literature, water molecules can be adsorbed in metal oxide films with various bonding states, including water molecules strongly bound to hydroxyl groups and hydrogen-bonded water molecules [38]. It was also shown that Hf–OH stretching vibrations can appear as a band at around 1575 cm^{-1} in the FT-IR spectrum of HfO_2-SiO_2 binary oxides, associated with water absorption and increase in OH [39]. Multiple weak peaks dispersed around this wavenumber are seen in the zoom-in FT-IR absorbance spectrum for the pristine device shown in

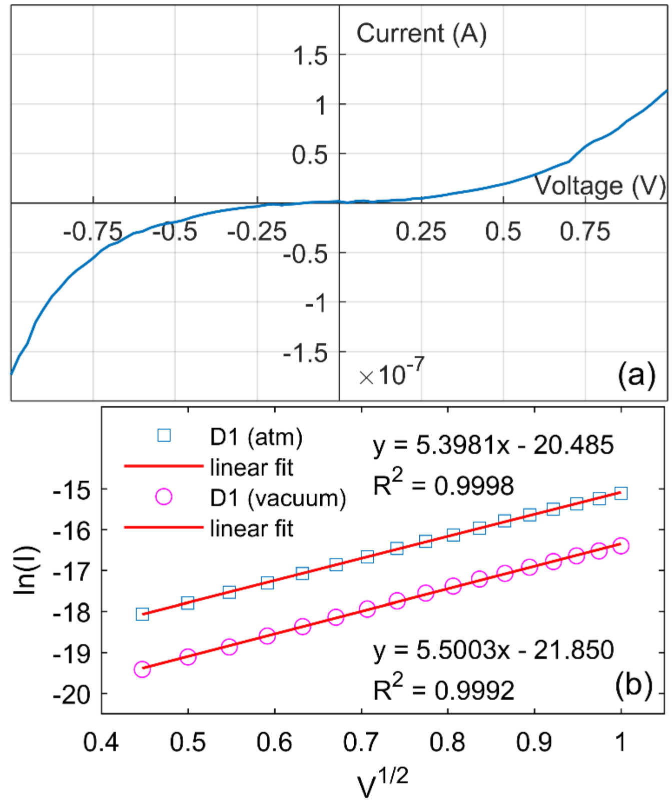

Fig. 6. (a) High resistance state (HRS) of Cu/HfO_2/p^+-Si devices exhibiting back-to-back Schottky diode characteristics. (b) Current–voltage relation in the HRS follows the Schottky emission.

Supplementary Material Fig. S7, whereas these are not visible in the spectrum of the vacuum-tested device. As suggested by this data, the desorption of water in the vacuum-tested device maybe forming a partially damaged hydroxyl-bond network, wherein the associated defects in the network act as electron traps at the grain boundries. These findings suggest that the defects generated due to the desorption of water, in addition to the presence of carboxylate groups (COO^-) and carbonate species, play a role in the electronic transport when the device is biased in vacuum, under the described biasing conditions.

D. Air Leak Detector Circuit Implementation

Fig. 7 shows the circuit implementation of the sensor prototype. The proposed portable, cost-effective, power-efficient, and easy-to-implement prototype consists of an Arduino Uno microcontroller (5 V and 16 MHz), a low pass filter (LPF), a resistor connected in series with the memristor, and a couple of LEDs to serve as pressure/leak indicators. The Arduino microcontroller is used to power and control the circuit. The LPF transforms the Arduino pulse width modulation (PWM) output to a constant DC supply (Vs) that is supplied to the circuit. The filter design parameters are selected to achieve adequate time response without affecting the output voltage (Vs). The potential difference across the MR (VM) is read through the Arduino analog input (A1). The resistor R_1 connected in series with the memristor provides a voltage reference and it is used to determine the value of the current I using (5):

$$I = \frac{V_s - V_m}{R_1} \tag{5}$$

TABLE II
COMPARISON BETWEEN THE PROPOSED WORK AND OTHER PRESSURE SENSORS REPORTED IN THE LITERATURE

Work	Sensor	Pressure range	Power	Sensor Area	Sensing Mechanism	Circuitry
[4]	Mechanical resonator	7.5 – 900 Torr	520 µW	350 x 130 µm^2	Mechanical	Sensor + Amplifier + Frequency Detector + Charge Pump + Filter + VCO
[5]	Piezoelectric beam structure	6.5 × 10^{-6} - 760 Torr	-	20 x20 mm^2	Mechanical	Sensor + Amplifier + Function Generator + Spectrum Analyzer
[6]	Surface acoustic wave	1x10^{-4} – 1x10^{3} Torr	-	7 x 5 mm^2	Mechanical	Sensor + Network Analyzer HP8752A
[7]	Ni resistor	1x10^{-5} – 1 Torr	0.5 mW	0.4 x 1 mm^2	Thermal	-
[8]	tungsten resistor	7.5x10^{-3} – 750 Torr	0.05 W	40 x 40 µm^2	Thermal	Sensor + Heater + Voltage Source + Amplifier + 8 Bit SAR A/D Converter
[9]	micro-Pirani	2.2x10^{-3} – 750 Torr	3.56 mW	200 x 200 µm^2	Thermal	-
[10]	Thermoelectric	1x10^{-2} – 10 Torr	-	800 x 800 um^2	Thermal	Sensor + Power Supply + Function Generator + Chopper and PLL Amplifiers + Filter
[11]	Pirani with hollow heater	0.8 – 200 Torr	180 µW	206 x 82 µm^2	Thermal	-
This work	**Memristor**	**4.9x10^{-5} -760 Torr**	**8 nW**	**2 x 2 mm^2**	**Electrical**	**Sensor + Arduino microcontroller + Low Pass Filter**

The value of R1 is selected to be 1 MΩ, which provides a suitable reference within the range of off-state resistance values of the sensor. The memristor resistance (RM) can be found by using (6):

$$R_M = \frac{V_M}{I} \quad (6)$$

As part of its programming scheme, the Arduino microcontroller can also be used to turn on some LEDs to provide leak state indication, as suggested in Fig. 7. In this scheme, the resistance of the memristor *RM* is measured periodically. While the percentage of change in the resistance remains within a predetermined range, the green LED is powered on and the other two LEDs are off, indicating that there is no significant leak. On the other hand, if the resistance starts increasing gradually, with a slope greater than a predetermined value, then the green LED is turned off and the blue LED is turned on, registering a considerable level of air leak. Finally, in the case of an abrupt change in the resistance, the red LED will switch on to mark that a critical leak state is reached. For instance, this indication level could be programmed to be at a resistance ratio of 2, where 83% of the experimentally recorded ratios lie above. The programming of the Arduino controller has been done in Arduino IDE. The complete Arduino code for the process is available on GitHub [40].

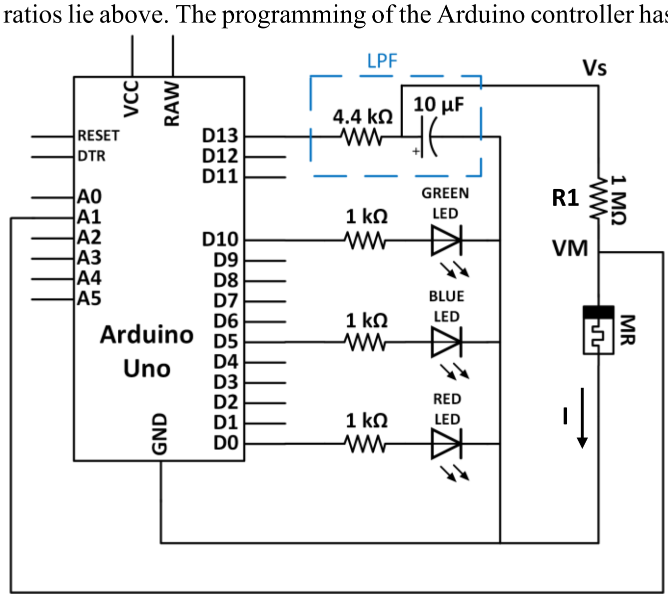

Fig. 7. Prototype implementation of the vacuum sensing system.

E. Comparison with Other Solutions

Table II provides a comparison between the proposed work and other existing pressure sensors in the literature. It can be observed that the proposed prototype reduces the power consumption by at least three orders of magnitude. Moreover, it provides a portable and easy-to-implement solution based on a commercially available single-board microcontroller, eliminating the need for bulky systems comprised of charge pumps, amplifiers, function generators, spectrum analyzers, and so on. In addition, the sensor does not depend on temperature or frequency changes, which makes it less susceptible to noise and interference [4].

IV. CONCLUSION

We present a novel, low-cost, and low-power vacuum pressure sensor based on 2 mm x 2 mm Cu/HfO_2/p^+-Si memristor devices. The off-state resistance of the device is found to be inversely proportional to the pressure when the pressure changes from atmospheric to vacuum. A sensitivity of 493 $Torr^{-1}$ was demonstrated by the sensor when working in the pressure range of 4.9x10^{-5} - 760 Torr. The power consumption of the system is in the nanowatt range (~ 8 nW), which is orders of magnitude small compared to the state-of-the-art implementations and is suitable for long lifetime devices. A portable prototype integrated on a single-board microcontroller is also presented. This may aid in solving critical challenges in leak detection in pressurized structures like space vehicles, by enabling the use of an array of many sensors without significant contributions to the payload and power consumption. The small area and light weight of the proposed sensing system can be further enhanced by an Application Specific Integrated Circuit (ASIC), substituting the Arduino microcontroller, in a system-on-chip design.

ACKNOWLEDGMENTS

This work is funded by the United Arab Emirates Space Agency, Space Missions Science and Technology Directorate, project reference K08-2016-001. The proposed project is in line with the United Arab Emirates Space Agency's Space Science, Technology and Innovation (ST&I) Roadmap which aims at developing enabling technologies for Space exploration that are intended to accomplish the objectives of the UAE Space Strategy. The authors also acknowledge the access granted to the System-on-Chip Centre (SoCC) that is supported by the Khalifa University (KU) award No. [RC2-2018-020], as well as the access granted to the electron microscopy suite through the KU-Research Laboratories, to achieve, respectively, the electrical and material characterization studies presented in this work. The authors acknowledge Dr. Anas Al Azzam for granting access to the MEMs Lab at KU to achieve the device fabrication. The authors declare that they have no conflicts of interest.

References

[1] C. Clark, L. Labonte, J. Castro, A. Abedi, and V. Caccese, "Wireless leak detection using airborne ultrasonics and a fast-Bayesian tree search algorithm with technology demonstration on the ISS," in *2015 IEEE International Conference on Wireless for Space and Extreme Environments (WiSEE)*, 2015, pp. 1-5.

[2] K. D. Champaigne and J. Sumners, "Wireless Impact and Leak Detection and Location Systems for the ISS and Shuttle Wing Leading Edge," in *2005 IEEE Aerospace Conference*, 2005, pp. 1-8.

[3] E. Christiansen, "Micrometeoroid and Orbital Debris (MMOD) Risk Overview," ed: NASA Tech-Brief, 2014.

[4] K. Allidina, M. A. Taghvaei, F. Nabki, P. Cicek, and M. N. El-Gamal, "A MEMS-based vacuum sensor with a PLL frequency-to-voltage converter," in *2009 16th IEEE International Conference on Electronics, Circuits and Systems - (ICECS 2009)*, 2009, pp. 583-586.

[5] B. Wang and C. Wu, "Development of wide pressure range vacuum senser using piezoelectric beam structure," in *2014 Symposium on Design, Test, Integration and Packaging of MEMS/MOEMS (DTIP)*, 2014, pp. 1-5.

[6] P. Nicolay *et al.*, "SAW pressure sensor for vacuum control applications," in *2009 IEEE International Frequency Control Symposium Joint with the 22nd European Frequency and Time forum*, 2009, pp. 106-109.

[7] M. Purahmad *et al.*, "A MEMS-based resistive vacuum gauge with voltage readout," in *2013 26th International Vacuum Nanoelectronics Conference (IVNC)*, 2013, pp. 1-2.

[8] L. Jinfeng, T. Zhen'an, and W. Jiaqi, "System on chip thermal vacuum sensor based on standard CMOS process," *Journal of Semiconductors,* vol. 30, p. 035004, 2009.

[9] M. Piotto, S. Del Cesta, and P. Bruschi, "A Compact CMOS Compatible micro-Pirani Vacuum Sensor with Wide Operating Range and Low Power Consumption," *Procedia Engineering,* vol. 168, pp. 766-769, 2016/01/01/ 2016.

[10] S. J. Chen and Y. C. Wu, "Dual Phase Modulation of CMOS-MEMS Vacuum Sensor," in *2019 IEEE Eurasia Conference on IOT, Communication and Engineering (ECICE)*, 2019, pp. 1-4.

[11] Y. Sun, K. Liang, C. Cheng, M. Lin, R. Chen, and W. Fang, "Performance improvement of CMOS-MEMS Pirani vacuum gauge with hollow heater design," in *2015 Transducers - 2015 18th International Conference on Solid-State Sensors, Actuators and Microsystems (TRANSDUCERS)*, 2015, pp. 1069-1072.

[12] B. J. Choi *et al.*, "High-Speed and Low-Energy Nitride Memristors," vol. 26, no. 29, pp. 5290-5296, 2016.

[13] B. Govoreanu *et al.*, "10×10nm² Hf/HfO<inf>x</inf> crossbar resistive RAM with excellent performance, reliability and low-energy operation," in *2011 International Electron Devices Meeting*, 2011, pp. 31.6.1-31.6.4.

[14] Y. Li *et al.*, "Anomalous resistive switching in memristors based on two-dimensional palladium diselenide using heterophase grain boundaries," *Nature Electronics,* vol. 4, no. 5, pp. 348-356, 2021/05/01 2021.

[15] M. A. Zidan, J. P. Strachan, and W. D. Lu, "The future of electronics based on memristive systems," *Nature Electronics,* vol. 1, no. 1, pp. 22-29, 2018/01/01 2018.

[16] T. Li, X. Bi, N. Jing, X. Liang, and L. Jiang, "Sneak-Path Based Test and Diagnosis for 1R RRAM Crossbar Using Voltage Bias Technique," in *Proceedings of the 54th Annual Design Automation*, Austin, 2017, pp. 1-6.

[17] N. Talati, S. Gupta, P. Mane, and S. Kvatinsky, "Logic Design Within Memristive Memories Using Memristor-Aided loGIC (MAGIC)," *IEEE Transactions on Nanotechnology,* vol. 15, no. 4, pp. 635-650, 2016.

[18] K. Humood, B. Mohammad, H. Abunahla, and A. Alazzam, "On-Chip Tunable Memristor-Based Flash Analog to Digital Converter for AI applications ," (in En), *IET Circuits, Devices & Systems,* vol. 14, pp. 107-114, 2019.

[19] A. Sebastian, M. Le Gallo, R. Khaddam-Aljameh, and E. Eleftheriou, "Memory devices and applications for in-memory computing," *Nature Nanotechnology,* vol. 15, no. 7, pp. 529-544, 2020/07/01 2020.

[20] S. A. Hadi, K. Humood, M. A. Jaoude, H. Abunahla, H. Shehhi, and B. Mohammad, "Bipolar Cu/HfO2/p++ Si Memristors by Sol-Gel Spin Coating Method and Their Application to Environmental Sensing," *Scientific Reports,* vol. 9, no. 1, p. 9983, 2019.

[21] I. Tzouvadaki *et al.*, "“Bio-functionalization study of Memristive-Biosensors for early detection of prostate cancer”," in *2015 11th Conference on Ph.D. Research in Microelectronics and Electronics (PRIME)*, 2015, pp. 17-20.

[22] S. Khandelwal, A. Bala, V. Gupta, M. Ottavi, E. Martinelli, and A. Jabir, "Fault Modeling and Simulation of Memristor based Gas Sensors," in *IEEE EEE 25th International Symposium on On-Line*

Testing and Robust System Design (IOLTS), Rhodes, Greece, 2019 pp. 58-59.

[23] K. Humood, S. Saylan, B. Mohammad, and M. Abi Jaoude, "Effect of the Compliance Current on the Retention Time of Cu/HfO2-Based Memristive Devices," *Journal of Electronic Materials,* 2021/05/11 2021.

[24] H. Jiang *et al.*, "A novel true random number generator based on a stochastic diffusive memristor," *Nature Communications,* vol. 8, no. 1, p. 882, 2017/10/12 2017.

[25] S. Saylan, H. Aldosari, K. Humood, M. Abi Jaoude, F. Ravaux, and B. Mohammad, "Effects of top electrode material in hafnium-oxide-based memristive systems on highly-doped Si," *Scientific reports,* vol. 10, no. 1, pp. 1-8, 2020.

[26] K. Humood, S. Saylan, M. Abi Jaoude, B. Mohammad, and F. Ravaux, "Impact of vacuum on the resistive switching in HfO2-based conductive-bridge RAM with highly-doped silicon bottom electrode," *Materials Science and Engineering: B,* vol. 271, p. 115267, 2021/09/01/ 2021.

[27] F. Pan, S. Gao, C. Chen, C. Song, and F. Zeng, "Recent progress in resistive random access memories: Materials, switching mechanisms, and performance," *Materials Science and Engineering,* vol. R 83, pp. 1–59, 2014.

[28] S. Menzel, U. Böttger, M. Wimmer, and M. Salinga, "Physics of the Switching Kinetics in Resistive Memories," *Advanced Functional Materials,* vol. 25, pp. 6306–6325, 2015.

[29] D. Ielmini, "Resistive switching memories based on metal oxides: mechanisms, reliability and scaling," *Semiconductor Science and Technology,* vol. 31, 2016.

[30] C. Sun, S. M. Lu, F. Jin, W. Q. Mo, J. L. Song, and K. F. Dong, "The Resistive Switching Characteristics of TiN/HfO2/Ag RRAM Devices with Bidirectional Current Compliance," *Journal of Electronic Materials,* vol. 48, no. 5, pp. 2992-2999, 2019/05/01 2019.

[31] X.-m. Wang *et al.*, "Sea urchin-like microstructure pressure sensors with an ultra-broad range and high sensitivity," *Nature Communications,* vol. 12, no. 1, p. 1776, 2021/03/19 2021.

[32] A. J. Chiquito, C. A. Amorim, O. M. Berengue, L. S. Araujo, E. P. Bernardo, and E. R. Leite, "Back-to-back Schottky diodes: the generalization of the diode theory in analysis and extraction of electrical parameters of nanodevices," *Journal of Physics: Condensed Matter,* vol. 24, no. 22, p. 225303, 2012.

[33] Z. Wang *et al.*, "Extraction and Analysis of the Characteristic Parameters in Back-to-Back Connected Asymmetric Schottky Diode," *physica status solidi (a),* vol. 217, no. 8, p. 1901018, 2020.

[34] S. Kasap and P. Capper, *Springer handbook of electronic and photonic materials*. Springer, 2017.

[35] Y. Hiruma, K. Yoshikawa, and M.-a. Haga, "Bio-inspired protonic memristor devices based on metal complexes with proton-coupled electron transfer," *Faraday discussions,* vol. 213, pp. 99-113, 2019.

[36] G. Milano *et al.*, "Water-mediated ionic migration in memristive nanowires with a tunable resistive switching mechanism," *ACS applied materials & interfaces,* vol. 12, no. 43, pp. 48773-48780, 2020.

[37] S. Porro *et al.*, "Multiple resistive switching in core–shell ZnO nanowires exhibiting tunable surface states," *Journal of Materials Chemistry C,* vol. 5, no. 40, pp. 10517-10523, 2017.

[38] T. Tsuruoka, K. Terabe, T. Hasegawa, I. Valov, R. Waser, and M. Aono, "Effects of moisture on the switching characteristics of oxide-based, gapless-type atomic switches," *Advanced Functional Materials,* vol. 22, no. 1, pp. 70-77, 2012.

[39] D. Neumayer and E. Cartier, "Materials characterization of ZrO 2–SiO 2 and HfO 2–SiO 2 binary oxides deposited by chemical solution deposition," *Journal of Applied Physics,* vol. 90, no. 4, pp. 1801-1808, 2001.

[40] Available: https://github.com/KhaledHumood/MemChar-Low-Power-and-Low-Cost-Arduino-Based-Characterization-Tool-for-Memristor-Devices

Khaled Humood is a PhD student at the Electronics and Computer Science, University of Southampton, Southampton, United Kingdom. Prior that, Khaled was a research associate at the Department of Electrical and Computer Engineering and System on Chip Center in Khalifa University, Abu Dhabi, United Arab Emirates. Khaled received his B.Sc and M.Sc. degree in Electrical and Computer Engineering from Khalifa University in 2017 and 2019, respectively. His research interests include VLSI, emerging technology such as RRAM, memory design, electrical characterization, in-memory computing and circuit design.

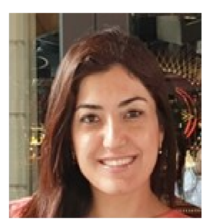

Dr. Sueda Saylan obtained her PhD in Interdisciplinary Engineering from Masdar Institute, Khalifa University's flagship sustainability-focused research institute, and has been working since 2016 at Khalifa University as postdoc, with research interests embracing memristor-based devices, opto-electronic devices, and light management by using micro/nano-scale structures. Dr. Saylan conducted research at prestigious labs, specifically the System-on-Chip Center (KU, UAE), Nano-Optics and Optoelectronics Research Laboratory (MI, UAE), Nakano and Tanemura Laboratory (UTokyo, Japan), and the Fitzgerald Group (MIT, USA).

Dr. Baker Mohammad (M'04-SM'13) earned his PhD from University of Texas at Austin in 2008, his M.S. degree from Arizona State University, Tempe, and BS degree from the University of New Mexico, Albuquerque, all in ECE. Baker is a System on Chip center director and a professor of EECS at Khalifa University. Before joining Khalifa University, he was a Senior Staff Engineer/Manager at Qualcomm, Austin, USA for 6-years, where he was engaged in designing high performance and low power DSP processor used for communication and multi-media application. Before joining Qualcomm, he worked for ten years at Intel Corporation on a wide range of microprocessors design from high performance, server chips > 100Watt (IA-64), to mobile embedded processor low power sub 1 watt (xscale). He has over 16 years of industrial experience in microprocessor design, emphasizing memory, low power circuit, and physical design. His research interests include VLSI, power-efficient computing, high yield embedded memory, emerging technology such as memristor, STTRAM, and In-Memory-Computing, hardware accelerators for Cyber-Physical systems. In addition, he is engaged in a microwatt range computing platform for wearable electronics and WSN focusing on energy harvesting, power management, and power conversion including efficient dc/dc, ac/dc convertors.

Baker authored/co-authored over 100 referred journals and conference proceedings, > 4 books, 18 US patents, multiple invited seminars/panelist, and the presenter of 3 conference tutorials including one tutorial on Energy harvesting and Power management for WSN at the 2015 (ISCAS). Baker is a associate editor for IEEE Transaction on VLSI (TVLSI), and microelectronics journal, Elsevier. Dr. Mohammad participates in many technical committees at IEEE conferences and reviews for journals including TVLSI, IEEE Circuits and Systems.

Dr. Maguy Abi Jaoude acquired her Ph.D. in Analytical Chemistry in 2011 from the University of Claude Bernard - Lyon 1. In 2012, she held an adjunct chemistry instructor position at the same institution, and in late 2013, she joined the Khalifa University of Science, Technology, and Research (KUSTAR) in Abu Dhabi, as Assistant Professor of Chemistry. Since Fall 2017, she has been with the Khalifa University of Science and Technology (KU), post-university merger, and is now Associate Professor at the Department of Chemistry and a member of the Center for Catalysis and Separations (CeCaS) and the Center for Membranes and Advanced Water Technology (CMAT). Her research program focuses on the development of hydrothermal and sol-gel synthesis methods for producing a range of exotic and hierarchically structured oxides of rare earth and transition elements, both at bulk scale and in situ. She is interested in tuning and understanding the structure-property relationships of low dimensional systems for application in advanced oxidation processes for environmental catalysis focusing on de-pollution technologies. Also, she has ongoing collaborations with the KU System on Chip Center (SoCC) where she explores the use of such materials for the development of emerging memory and environmental sensing devices.